JLAB-PHY-99-27

Physics with CLAS

Elton S. Smith for the CLAS Collaboration [a] *

[a]Jefferson Lab, Newport News, Va. 23606, USA

Abstract. We describe the physics program and the experimental equipment of the CEBAF Large Acceptance Spectrometer, CLAS. The spectrometer is located in Hall B, one of the three experimental areas at the Continuous Electron Beam Accelerator Facility (CEBAF) operated by the Thomas Jefferson National Accelerator Facility. We review the program to study baryon resonances to demonstrate the multi-particle detection capabilities of the CLAS detector.

1. Introduction

The Thomas Jefferson National Accelerator Facility (Jefferson Lab) is a superconducting electron accelerator which delivers a low-emittance, high resolution, 100% duty-cycle electron beam to three different experimental areas simultaneously. Presently, the maximum beam energy is 5.6 GeV, with a maximum current of 180 μA. Polarized beams of up to 60 μA at 80% polarization are routinely available.

The CEBAF Large Acceptance Spectrometer (CLAS) at Jefferson Lab is a unique facility designed to accommodate a very broad spectrum of physics measurements [1]. The spectrometer is optimized for characterizing multiple particle final states over a wide kinematical range, with good momentum and angular resolution, and neutral and charged particle identification. Physics measurements have been performed with numerous combinations of targets, magnetic field settings, and beam energies, using photon and electron beams; more than nine billion triggers have been acquired to date. Targets include polarized and unpolarized cryogenic liquids, and solids. The spectrometer contains six independently instrumented sectors, which in combination with Møller electron shielding allows it to withstand relatively high luminosities (10^{34} cm^{-2}s^{-1}). A fast, distributed data acquisition system in combination with a highly configurable two-level trigger scheme permits data acquisition rates of up to 3 kHz with good event selectivity, producing up to half a terabyte of data per day.

The baryon physics program being carried out with CLAS includes studies of electromagnetic transition form factors of resonances, searches for exotic and missing states, asymmetries and sum rule studies, and hyperon production and decay, all in exclusive channels. Several analogous studies are being performed on nuclei, as well as studies of correlated multinucleon emission, measurements of nuclear transparency, and inclusive electron scattering on nuclei. The broad and continuous range in Q^2 and W accessible to

*Presented at the III Latinamerican Workshop on Nuclear and Heavy Ion Physics, San Andres, Colombia, September 13-17, 1999.

CLAS permits physics measurements of unprecedented quality in these experiments. To date, CLAS has a total of 59 approved experiments.

2. Spectrometer Components

The CLAS consists of a large open-geometry six-coil superconducting magnet producing a toroidal magnetic field, three separate drift chamber assemblies, a threshold Cerenkov counter, multi-purpose electromagnetic shower calorimeters, and a complete coverage of time-of-flight scintillation counters. In addition, there is a bremsstrahlung photon tagging facility for photon beam experiments.

The superconducting magnet produces a maximum integrated magnetic induction of 2.7 T-m at forward angles, decreasing to 0.5 T-m at larger angles. Its geometry provides an unobstructed solid angle range of more than half of 4π, and essentially all detector support structure and on-board electronics is mounted in the 'shadow' of the coil cryostat, preserving the unobstructed volume. Besides the superconducting magnet, there is a small normal-conducting magnet producing a toroidal field immediately surrounding the target region for magnetic shielding of Møller electrons. This geometry preserves the zero-field region around the target as well as in the first drift chamber region.

The drift chambers are divided into 3 concentric 'regions'; Region 1 surrounds the target, Region 2 is in the full magnetic field region, and Region 3 is in the outermost (low field) region. Thus the directions of the charged particles are determined before, during, and after bending. In total there are 35,148 sense wires arranged in an hexagonal cell geometry. Each region has two sets of wires ('superlayers'). The 'axial' superlayers are perpendicular to the beam axis and measure the polar angle of the track, while the 'stereo' superlayers are oriented at 6 degrees to measure the azimuthal angle. The total number of wire layers is 34. The chambers subtend polar angles from 8 to 142 degrees.

The intrinsic position resolution of the drift chamber system has been demonstrated to be approximately 200 μm in a given cell; in practice, 350-400 μm has been achieved for the overall system. This value is limited by the quality of detector alignment and calibrations, which are gradually improving. The momentum resolution achievable at lower particle momenta (<2.5 GeV) is completely dominated by multiple scattering through the 0.6-1 g/cm^2 thickness of the combination of target cell, gas window, and chamber gas. For higher particle momenta, the intrinsic position resolution dominates the momentum resolution, which is $< 1\%$. Vertex resolutions of 2.0 mm have been achieved; angular resolutions are currently limited to 10 mradians due to systematic uncertainties. Occupancies in the drift chambers for typical electron beam experiments range from 1 - 3%, while for photon beam experiments they are even smaller.

The electromagnetic shower calorimeters are lead-scintillator sampling calorimeters 16 radiation lengths thick. In total there are 1808 electronic channels. They subtend a polar angle range of 8 - 45 degrees in four sectors, and 8 - 70 degrees in two sectors. They are constructed in a projective geometry to maximize position resolution for neutral particles, and are segmented longitudinally into two submodules for improved electron-pion discrimination. The pion rejection factor is approximately 100:1 for a 95% electron detection efficiency. The intrinsic energy resolution for showering particles is $10\%/\sqrt{E}$, with approximately a 3 cm position resolution at 1 GeV. These detectors have up to 60%

efficiency for detecting high momentum neutrons. Because they have better than half-nanosecond intrinsic timing resolution, neutron-photon discrimination may be performed, as well as measurement of the neutron momentum.

The threshold Cerenkov counter array uses C_4F_{10} gas, which has a pion threshold of 2.8 GeV. The light is collected via an array of ultralight hyperbolic and elliptical mirrors which focus rays into a Winston cone in front of a 5" photomultiplier tube with typically 2 or 3 reflections. In total there are 216 phototubes. The detector is located 4 m from the target, and subtends polar angles from 8 to 45 degrees and azimuthal angles within each sector of ± 25 degrees. The average number of photoelectrons per electron ranges from 8 to 10; the threshold is typically set to 0.2 photoelectrons. The electron efficiency can be systematically measured during routine data taking using elastic e-p scattering. It is typically better than 99% in the fiducial regions.

The time-of-flight scintillators are fabricated from BC-408, 5 cm thick, and subtend the full range of angles covered by the drift chambers. 342 separate detectors are read out from both ends. They have an intrinsic timing resolution ranging from 60 to 160 ps, depending on the detector length; in practice, 140 ps has been obtained as an average value for electrons under normal running conditions.

The Level 1 trigger can incorporate signals from the calorimeters, Cerenkov counters, time-of-flight counters, and the bremsstrahlung tagging system. The Level 2 trigger incorporates track information from the drift chambers.

3. Spectrometer Performance

A typical event is shown in Figure 1. The channel shown is $ep \rightarrow e'\pi^+\pi^-p$. The view shown in Figure 1a consists of a horizontal slice through the middle of the detector, while Figure 1b is a vertical slice through the detector, perpendicular to the beamline, at the target location.

Typical running conditions for electron beam experiments include: a 10 nA beam on a 5-cm liquid hydrogen target, resulting in a Møller electron rate of approximately 10^9 Hz, an hadronic production rate of approximately 10^6 Hz, and a trigger rate of 2 - 3 kHz with a 10% dead time, using a single electron trigger (a Cerenkov counter hit and the calorimeter energy sum above threshold). Data rates to disk are typically 10 Mbytes/s. The electron selectivity varies widely, depending on the beam energy and trigger selection. Using the Level 1 trigger it averages from 40 - 50%, improving significantly when the Level 2 trigger is also employed.

Typical conditions for photon beam experiments: 10^7 tagged photons per second incident on a 18 cm cryogenic target cell, resulting in a trigger rate of 2-3 kHz, dead times of 10%, and an accidental rate ranging from 25 - 50% (reduced to a few percent after off-line analysis).

Charged particle identification is performed by the time-of-flight technique, resulting in very well separated pions and protons, and a 5:1 peak-to-background ratio for kaons. Neutral particle identification is accomplished in the electromagnetic shower calorimeter, where time-of-flight is used to distinguish photons from neutrons, and to calculate neutron momentum.

Missing mass resolutions of 10 - 20 MeV have been demonstrated for, e.g., electropro-

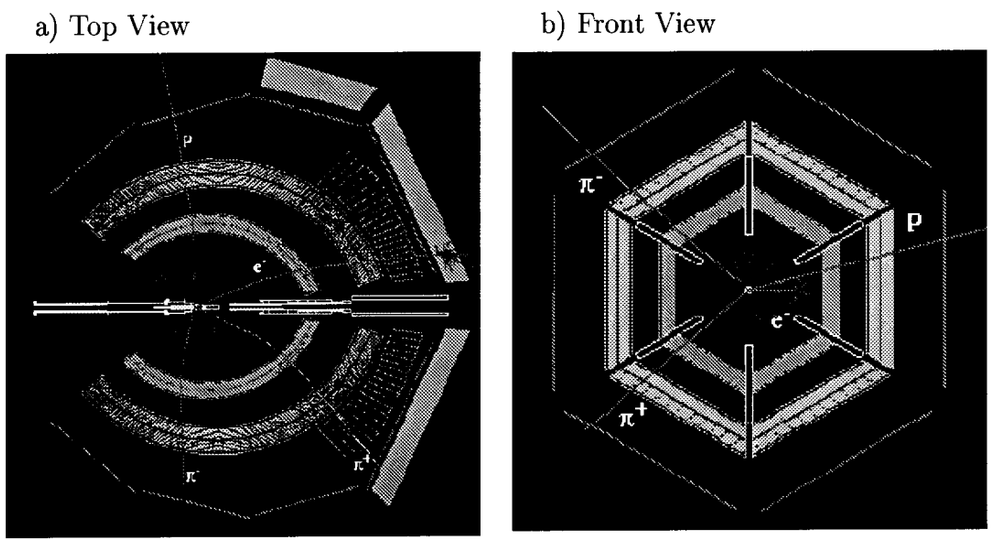

Figure 1. The reaction $ep \rightarrow e'\pi^+\pi^- p$ is shown in CLAS.

duced Λ, Σ°, η, and ω from the proton with a 4 GeV beam. See Figure 2 for an example of the missing mass spectra from the reactions $ep \rightarrow epX$, and $ep \rightarrow e\pi^+X$. The resolution improves for lower beam energies, as seen in both photoproduction and electroproduction.

4. Physics Program

A wide variety of measurements has already been carried out using CLAS in the first twenty months of operation. The data acquisition is organized by 'run periods,' where experiments which share common running conditions take data simultaneously. These run periods include ('h' = charged hadron, X = anything):

g5: photofission total cross section on heavy nuclei; data taking completed, analysis underway.

e1a: $e + p \rightarrow e' + X$ (13 experiments); 3 complete analysis passes finished.

g1a,b: $\gamma + p \rightarrow h + X$ (6 experiments); first analysis pass completed for g1a.

g6a,b: $\gamma + p \rightarrow \phi(1020) + X$, $\gamma + p \rightarrow hh + X$ (2 experiments); data taking completed, g6a first analysis pass complete.

eg1: $\vec{e} + \vec{p}(\vec{D}) \rightarrow e' + X$ (4 experiments); first pass analysis nearing completion.

e1b: $\vec{e} + p \rightarrow e' + X$ (13 experiments); calibration complete, first analysis pass beginning.

e2: $\vec{e} + {}^3He,\ {}^4He,\ Fe \rightarrow e' + X$ (8 experiments); analysis is underway.

g2a: $\gamma + D \rightarrow h + X$ (4 experiments); data taken.

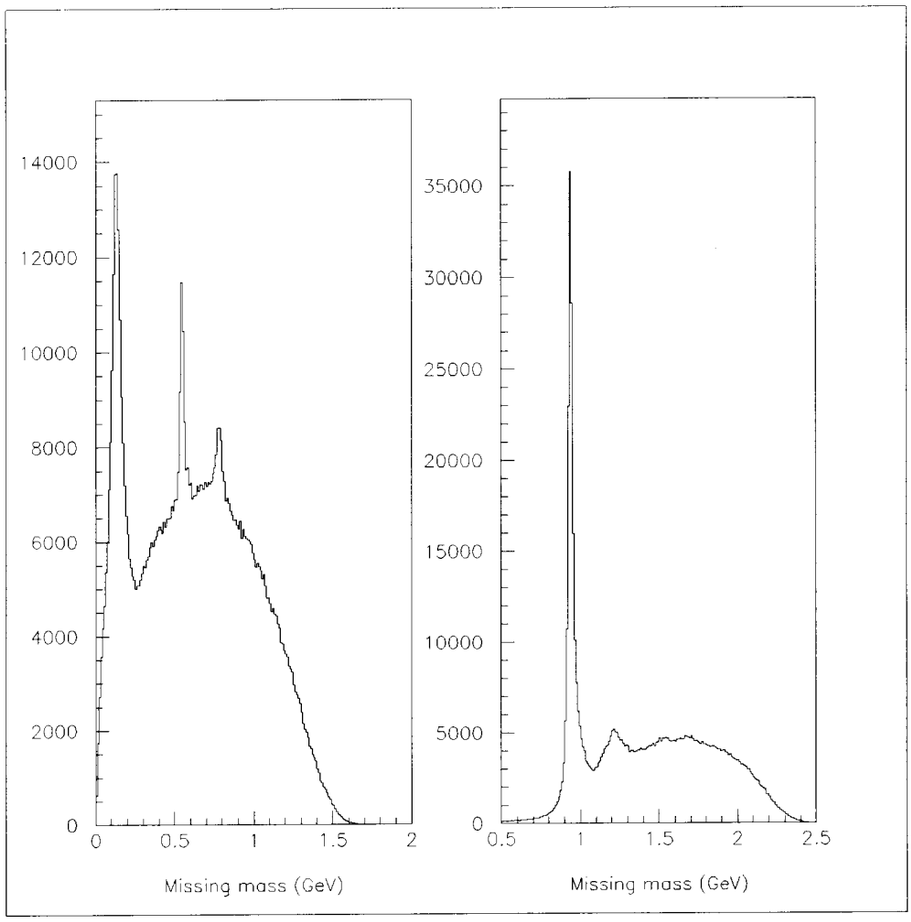

Figure 2. Missing mass for $ep \to epX$ (left), and $ep \to e\pi^+X$ (right). The peaks correspond to the π^o, η, ρ/ω, and neutron mass, respectively.

The data calibration and analysis passes are performed at Jefferson Lab on the off-line compute farm, which is presently equipped with 115 fast CPU's; further expansion is planned.

5. Electromagnetic Excitation of Baryon Resonances

To demonstrate the capabilities of the CLAS detector, we review the program to study baryon resonances, or N^* program [2,3,4]. The goal of the N^* program (N^* is here used for N and Δ states) is to probe the internal structure of light quark baryons. This is accomplished in various way: (1) by studying the resonance transition form factors over a large Q^2 range and for a large number of states. This allows detailed tests of baryon structure models and probes the contributions from hard and soft processes (2) by searching for the so-called "missing resonances", states which are predicted in the

symmetric quark model but have not been seen so far, and (3) by searching for gluonic excitations of the nucleon ("hybrid baryons").

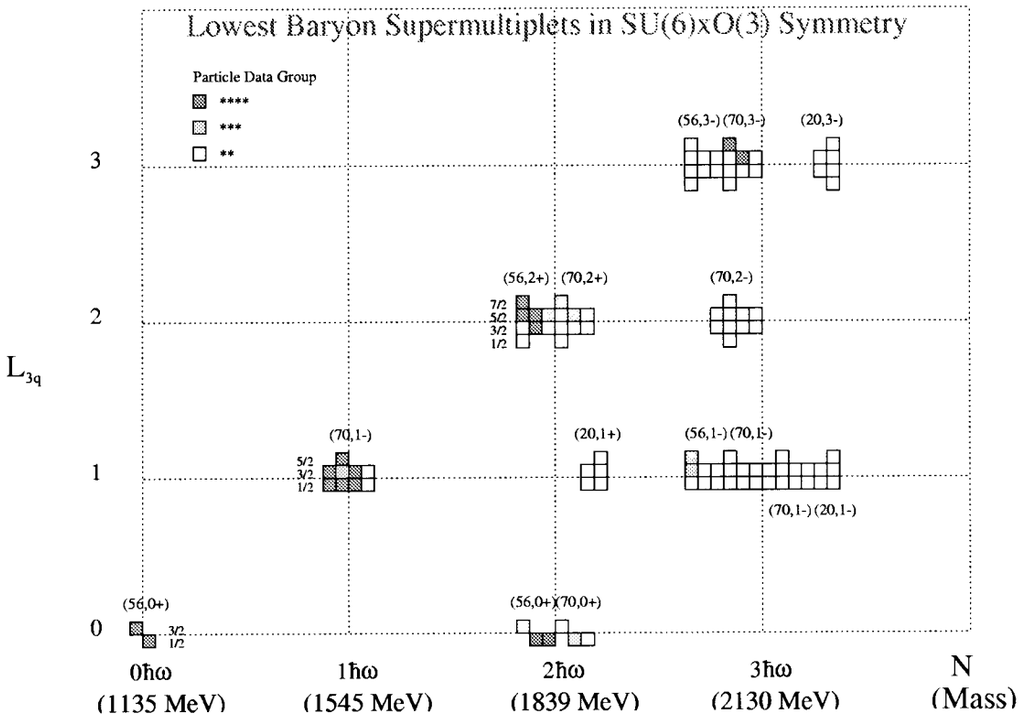

Figure 3. Excited nucleon states predicted in the symmetric quark model. Empty boxes represent states which are expected, but have not been observed.

The constituent quark model[5,6] (CQM) predicts a large number of resonant light quark (u,d,s) baryon states within the symmetry group $SU(3)_{flavor} \otimes SU(2)_{spin} \otimes O(3)_{space}$. The states fall into supermultiplets with fixed orbital angular momentum and energy excitation level. The mass degeneracy within one supermultiplet is broken by the color magnetic hyperfine coupling between the quark spins. The predicted spectrum is shown in Figure 3.

5.1. Total Absorption Cross Section

The total photon absorption cross section exhibits 3 or 4 enhancements associated with the excitation of some of the prominent resonances - the $\Delta^+_{\frac{3}{2}}(1232)$, $N(1520)$, $N^+_{\frac{5}{2}}(1680)$, and $\Delta^+_{\frac{7}{2}}(1950)$. From inclusive measurements we obtain only global information about the resonance form factors, and even this is only true in the region of the Δ resonance, a relatively isolated state. The higher mass states overlap, and since they have several hadronic decay channels open they are broad and do not appear as isolated states in the inclusive spectrum. Three states contribute to the enhancement around 1.5 GeV, at least

seven to the bump at 1.7 GeV, and at least six are known in the mass region around 1.9 GeV. Many more are predicted with masses near 2 GeV.

The various states can only be separated if the hadronic final states are measured, e.g. $N\pi, N\eta, N\pi\pi$. Spin, parity and isospin of the intermediate state can be identified, and, using information on the hadronic decay vertex, the transverse ($\lambda_{\gamma N} = \frac{1}{2}, \frac{3}{2}$) and scalar ($\lambda_{\gamma N} = \frac{1}{2}$) electromagnetic transition amplitudes $A_{\frac{1}{2}}$, $A_{\frac{3}{2}}$, and $S_{\frac{1}{2}}$ can be determined and compared to model predictions. So far only single pion and single eta photo- or electroproduction data have been used in analyses. The CLAS program is aimed at improving this situation quantitatively as well as qualitatively. In Figure 4 we show the decomposition of the total cross section into a variety of final states using CLAS.

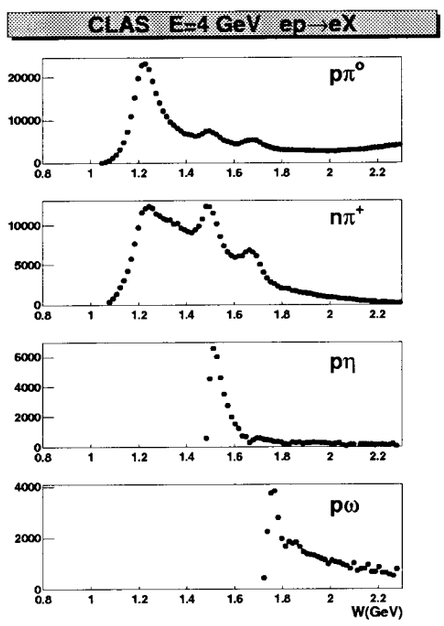

Figure 4. Yields for various channels measured with CLAS. The statistical error bars are smaller than the data points.

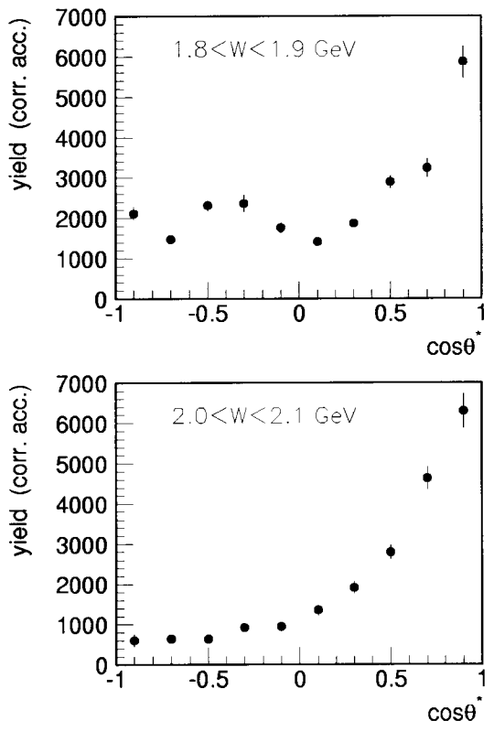

Figure 5. Electroproduction of ω mesons for different W bins. The deviation of the $\cos\theta$ distribution from a smooth fall-off for the low W bin suggests significant s-channel resonance production.

5.2. The $\gamma_v p\Delta(1232)$ Transition

The lowest $I = \frac{3}{2}$ state is the $\Delta(1232)$, which may be excited by a magnetic dipole transition or through electric and Coulomb quadrupole transitions. In the symmetric quark model model, a spin-flip in the ground state mediates the excitation. Dynamical

model give small values for $R_{EM} = \frac{E_{1+}}{M_{1+}}$. However, chiral invariance requires $R_{EM} \to 1$ for $Q^2 >> M^2$. Existing electroproduction data have large systematic uncertainties.

Several CLAS experiments focus on the precise measurement of the multipoles for the $\Delta(1232)$ over a large Q^2 range, by measuring the unpolarized differential cross section for charged and neutral pion production: $ep \to e'p\pi^0$, $ep \to e'n\pi^+$, and $en \to e'p\pi^-$, with high statistics, and by covering the full azimuthal and polar angular ranges. The quadrupole contributions can be detected in distortions of the pion angular distribution. Also, detailed measurements of polarization observables are in preparation.

5.3. "Missing" Quark Model States

The symmetric quark model predicts many states with masses above 1.8 GeV which have not been observed in $\pi N \to \pi N$ reactions (see Figure 3). Many of the "missing" states are predicted to decouple from the πN channel, however, they may couple to channels such as ρN, ωN, or $\pi\Delta$. Some may also couple to photons. Electromagnetic production of these channels may therefore be the only way to search for the "missing" states. Obviously, our picture of baryon structure could change dramatically if these states do not exist. Production of vector mesons or $\Delta^{++}\pi^-$ should provide a definite answer regarding the existence of at least some of these states [7]. For example, at forward angles the process $\gamma p \to p\omega$ is dominated by diffractive production, while resonance contributions would dominate at large angles. In electroproduction one expects the diffractive contribution to be reduced relative to the resonance contribution due to the increasing virtuality of the vector meson propagator involved.

Figure 5 shows preliminary data from CLAS in ω production on protons. The process is expected to be dominated by diffraction-like π° exchange with strong peaking at forward ω angles, or low t, and a monotonic fall-off at large t. The data show clear deviations from the smooth fall-off for the W range near 1.9 GeV, where some "missing" resonances are predicted, in comparison with the high W region [8]. Although indications for resonance production are strong, analysis of more data and a full partial wave study are needed before definite conclusions may be drawn.

5.4. Gluonic Excitations of the Nucleon

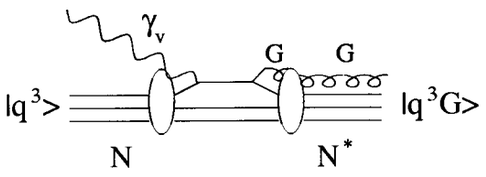

Figure 6. QCD Compton production of a gluonic excitation |q³G>.

In the past decade there have been speculations about the existence of gluonic baryon states $|q^3G>$ consisting of three constituent quarks and constituent glue[9,10] . QCD lattice simulations indicate that such configurations must exist for mesons, whereas no such calculations have been performed for baryons. Estimates within the framework of QCD sum rules [11] yield masses for the lowest gluonic baryon state P_{11}^G around 1.5 GeV.

Unfortunately, gluonic baryons cannot be distinguished from ordinary $|q^3>$ states

in hadronic production because they are, unlike some gluonic mesons, characterized by quantum numbers which are also possible for the normal $|q^3>$ baryon states. However, as their internal structure must be quite different from ordinary baryons, measurement of their transition form factors in electroproduction could be a powerful tool in these studies. A study of the Roper states $N_{\frac{1}{2}}(1440)$ and $\Delta_{\frac{3}{2}}(1600)$ as radial excitations of the 3-quark system or as gluonic excitation shows the transition form factors may be quite different for these alternative models. Moreover, because gluons have only transverse excitation modes, the longitudinal coupling is absent for gluonic excitations, and $S_{\frac{1}{2}}(Q^2) \equiv 0$.

6. Conclusions and Outlook

CLAS is operating well and has met all its essential design goals. The study of photo- and electroproduction of pseudoscalar and vector mesons from nucleons, provides rich information on the excitation of N^* and Δ resonances, their structure, and the strong interaction force in the non-perturbative regime. The utilization of state-of-the-art experimental equipment and data processing techniques has opened up the unique opportunity to collect the data needed for a comprehensive study of the structure of the nucleon in the confinement regime. CLAS started to take data related to the N^* program in December 1997. The analysis is progressing rapidly, and more data taking is scheduled for the year 1999 and 2000.

Acknowledgements

I would like to thank W. Brooks and V. Burkert for substantial contributions to the present text, and the organizers of the conference and the NSF Americas program for support of the session on the "Physics with Jefferson Lab." This work was supported in part by DOE Contract #DE-AC05-84ER40150.

REFERENCES

1. V. Burkert and B. Mecking, *Large Acceptance Detectors for Nuclear Physics*, in: *Modern Topics in Electron Scattering*, eds. B. Frois, I. Sick, *World Scientific, Singapore, 1991*
2. V. Burkert, *Leptonic Production of Baryon Resonances*, in *Perspectives in the Structure of Hadronic Systems*, eds. M.N. Harakeh *et al.*, *Plenum Press, New York, 1994*
3. V. Burkert, *Few-Body Systems Suppl. 11, 1 (1999)*
4. V. Burkert, preprint hep-ph/9910258, presented at PANIC99, Uppsala, Sweden, June 10 – 16, 1999; references therein.
5. N. Isgur, G. Karl, *Phys. Lett. 72B, 109 (1977); Phys. Rev. D23, 817 (1981)*
6. S. Capstick, N.Isgur, *Phys. Rev. D36, 2800 (1987)*
7. M. Ripani, presented at PANIC99, Uppsala, Sweden, June 10 – 16, 1999.
8. J. Manak, presented at PANIC99, Uppsala, Sweden, June 10 – 16, 1999.
9. T. Barnes, F.E. Close, *Phys. Letts. 123B, 89 (1983)*
10. E. Golowich, E. Haqq, G. Karl, *Phys. Rev. D28, 160 (1983)*
11. L. Kisslinger, talk presented at the CEBAF/INT Workshop on N^* physics, Seattle, Washington, September 9 - 13, 1996.